Chinese Chemical Letters 37 (2026) 111564

Contents lists available at ScienceDirect

Chinese Chemical Letters

journal homepage: www.elsevier.com/locate/cclet

Recent advances in polyoxometalate-based functional materials for sustainable remediation of radionuclide and heavy metal pollution

Yayu Dong[a], Jinghan Hao[b], Yingcai Wang[b], Xiaohong Cao[b], Zhimin Dong[b,d,*], Zhibin Zhang[b,*], Yunhai Liu[c,*]

[a] School of Materials Science and Engineering, East China Jiaotong University, Nanchang 330013, China
[b] State Key Laboratory of Nuclear Resources and Environment, East China University of Technology, Nanchang 330013, China
[c] Gandong University, Fuzhou 344000, China
[d] Institute of Nuclear Fuel and Nuclear Chemical Engineering, East China University of Technology, Nanchang 330013, China

ARTICLE INFO

Article history:
Received 10 June 2025
Revised 8 July 2025
Accepted 8 July 2025
Available online 9 July 2025

Keywords:
Polyoxometalates
Radionuclide
Heavy metal ions
Removal
Mechanisms

ABSTRACT

The severe threat of heavy metal pollution to ecological sustainability and human health has made the urgent development of efficient and environmentally friendly remediation technologies a necessity. Polyoxometalates (POMs), a class of unique metal-oxygen clusters with regulable structures and excellent properties, have emerged as promising candidates for removal of heavy metal ions. This review summarized the recent advances in POM-based functional materials (*e.g.*, host-guest, heterojunction, and POM-based metal-organic frameworks) for heavy metal ion remediation (such as U(VI), Pb(II), and Cr(VI)). The removal mechanisms, including adsorption, chemical reduction, photocatalytic reduction, adsorption-photocatalysis synergy, as well as the chemical sensor or probe for heavy metal detection, have been highlighted. Additionally, the challenges in improving material recyclability, scaling up synthesis, and understanding the long-term environmental impact of POMs are identified, while future research directions toward sustainable, cost-effective, and multifunctional POM-based systems are proposed. This review provides a comprehensive overview of POM-based functional materials potential in addressing heavy metal pollution, offering insights for designing next-generation environmental remediation materials.

© 2026 Published by Elsevier B.V. on behalf of Chinese Chemical Society and Institute of Materia Medica, Chinese Academy of Medical Sciences.

1. Introduction

Heavy metal pollution, accumulating in ecosystems through industrial discharges, mining activities, and agricultural practices, has emerged as a major global environmental issue drawing substantial attention due to the high toxicity, non-biodegradability, and bio-accumulation characteristics of heavy metal ions [1–13]. Even at very low concentrations, heavy metals such as chromium (Cr) and lead (Pb), can inflict serious damage on human health and the ecological environment [14–17]. These heavy metals can disrupt the normal physiological functions of organisms, damage vital organs, and even lead to chronic diseases and genetic mutations [18,19]. In addition to common heavy metals, radionuclides like uranium (U) and americium (Am) are widely acknowledged as global environmental contaminants, primarily owing to their inherent radioactivity and chemical toxicity [20–24]. The development of uranium enrichment strategies is of great significance for maintaining the sustainability of nuclear energy and advancing environmental governance. Therefore, the effective removal of heavy metal ions from wastewater is vital for environmental protection and human health.

Recently, substantial efforts have been directed toward developing efficient strategies, such as adsorption, chemical precipitation, photocatalytic/electrochemical treatment, and ion exchange [25–29], to address radionuclide and heavy metal pollution from the perspective of environmental sustainability. Among these approaches, functional materials play a pivotal role in enabling selective pollutant capture, enhancing treatment efficiency, and ensuring recyclability due to their unique structural and chemical properties. This dual emphasis on performance and sustainability highlight the need for rational material design and green synthesis methodologies, which are critical for optimizing functional materials for practical applications in radionuclide and heavy metal remediation. Common functional materials for heavy metal ions removal can be categorized into the following key types, each designed to address specific remediation needs: (1) Carbon-based

* Corresponding authors.
E-mail addresses: 202163003@ecut.edu.cn (Z. Dong), zhbzhang@ecut.edu.cn (Z. Zhang), Walton_liu@163.com (Y. Liu).

https://doi.org/10.1016/j.cclet.2025.111564
1001-8417/© 2026 Published by Elsevier B.V. on behalf of Chinese Chemical Society and Institute of Materia Medica, Chinese Academy of Medical Sciences.

materials, such as graphene, carbon nanotubes [30–32]. These materials can remove various heavy metal ions through physical and chemical adsorption due to their large specific surface area and simple preparation. However, they suffer from poor selectivity, low adsorption efficiency for trace heavy metals, and insufficient stability under acidic conditions. (2) Inorganic minerals, including montmorillonite, zeolites, metal oxides [33,34]. Although they usually exhibit high chemical stability and excellent ion-exchange selectivity, the relatively low adsorption capacity and agglomeration limit their further application in removal of heavy metal ions. (3) Organic polymer, such as ion-exchange resins, hydrogel, chitosan [35,36]. This type of material is characterized by abundant functional groups, with chitosan demonstrating good biocompatibility and resins having high exchange capacity. However, they exhibit poor acid resistance and are prone to degradation at high temperatures. (4) Porous crystalline materials [37–42]. Metal-organic framework (MOFs), covalent organic frameworks (COFs) are typical representative, which feature tunable pore structures and high specific surface area. Additionally, they can be easily functionalized by introducing specific adsorption sites, showing high selectivity for certain heavy metals. However, the frameworks are prone to decomposition under acidic conditions. (5) Bio-adsorbents [43–45], such as microbes, cellulose-based materials, which are derived from natural and renewable sources (plants, bacteria and algae). Therefore, bio-adsorbents show sustainability, environmental friendliness, biocompatibility, high surface area and versatile surface chemistry. As for the application, the selection or design of functional materials should integrate high efficiency and cost-effectiveness, tailored to the wastewater composition, treatment scale, and specific properties of target metal ions.

Among the numerous functional materials, polyoxometalates (POMs), defined as metal-oxygen clusters formed by early transition metals (*e.g.*, W, Mo, V) and oxygen, exhibit distinct properties of structural diversity, adjustable REDOX capacity, and unique active lattice oxygen [46–49]. POMs have found extensive applications across diverse fields, including optics, magnetism, catalysis, energy, and life sciences [50–57]. Recently, POMs have also been proven to be an ideal candidate in the field of removing heavy metal ions, which exhibit multi-dimensional advantages that are closely related to their unique structural characteristics, chemical properties, and functional designs. Despite significant advancements, a holistic overview integrating the dual functions of POMs in direct heavy metal ion capture and comprehensive environmental decontamination remains elusive.

This review endeavors to systematically synthesize the latest research on POM-based functional materials for heavy metal ion remediation. By dissecting the underlying mechanisms of adsorption, redox reactions, photocatalytic reduction, and synergistic processes, this review elucidates the structure-activity relationships critical for targeted heavy metal removal. Furthermore, it critically evaluates the advantages and challenges associated with POM-based functional materials and provides a forward-looking analysis of future research directions. Through this comprehensive examination, this review aims to offer robust theoretical foundations and practical guidelines for the large-scale application of POM-based functional materials in treating heavy metal-contaminated water.

2. Advantages of POM-based functional materials in the removal of heavy ions

POM-based functional materials demonstrate distinct advantages in heavy metal ion removal, featuring high efficiency, superior selectivity, and remarkable stability. These advantages are enabled by rational structural engineering strategies, including metal substitution, ligand modification, and cluster assembly. Their core competitiveness lies in the precise design of molecular structures and the integration of unique physicochemical properties, thus providing sustainable solutions for environmental remediation and related ecological sectors.

2.1. Structural diversity and functional adjustability

On the one hand, the molecular structure of POMs can be exquisitely tailored by manipulating the metal ions (W, Mo, V), organic ligands, and coordination modes, providing a design basis for the targeted removal of specific heavy metal ions [58]. On the other hand, POMs can be synergistically integrated with diverse functional materials, including covalent organic frameworks (COFs), graphene, perovskite, and metal-organic frameworks (MOFs) [59–64]. Through such strategic hybridization, the active sites of POMs can be combined with the high specific surface area/porous structure of these platforms, thereby enhancing adsorption capacity and mass transfer efficiency.

2.2. Multiple synergy action mechanisms

POM-based functional materials are capable of achieving removal efficiency for heavy metal ions *via* the synergistic interplay of multiple mechanisms. (1) Coordination complexation and ion exchange [65–67]. The terminal oxygen and bridge oxygen atoms, organic groups in POMs, can serve as coordination sites to form stable coordination bonds with heavy metal ions (U(VI), Pb(II)). Meanwhile, the exchangeable cations on the material surface (such as Na^+, K^+) can undergo ion exchange with heavy metal cations. (2) Redox and photocatalytic reduction. The metal ions of POMs (such as W^{6+}/W^{5+}, Mo^{6+}/Mo^{5+}, V^{5+}/V^{4+}) can reversibly transform between different oxidation states, forming stable REDOX pairs, which could be used to reduce toxic high-valent ions (such as Cr(VI), U(VI), Hg(II)) to low-toxicity or easily precipitated low-valent ions [68–70]. (3) Electrostatic attraction and adsorption-catalysis synergy [71,72]. The negatively charged surface of POMs exerts strong electrostatic attraction toward positively charged heavy metal cations. When combined with photocatalytic or chemical reduction processes, this synergy enables an integrated "adsorption-immobilization-conversion" mechanism, thereby significantly enhancing the removal efficiency.

2.3. High selectivity and environmental adaptability

POMs, as nanoscale metal-oxygen clusters, exhibit remarkable structural designability stemming from the high tunability of framework composition, spatial configuration, and assembly modes, thereby providing a unique platform for function-oriented material design [73]. On the one hand, classical POMs (such as $[PW_{12}O_{4n}]^{3-}$, $[PW_9O_{34}]^{9-}$) pose highly negative surface charges and abundant W-O/Mo-O groups, which exhibit strong electrostatic attraction toward high-valent cations (*e.g.*, U(VI) and Pb(II)) through electrostatic attraction. Moreover, distinct functional groups demonstrate differential affinity toward various heavy metal ions, governed by their coordination chemistry, steric characteristics and competitive capacity [37]. For example, surface modification of POMs through organic ligands with specific functional groups (*e.g.*, organic amines, thiols, phosphate groups) significantly enhances their coordination affinity toward specific metal ions, enabling targeted chelation *via* lone-pair electron donation.

On the other hand, when POMs are composited with other materials (*e.g.*, MOFs, COFs, or perovskites) to form hierarchical porous architectures, the precisely engineered pore dimensions enable size-exclusive targeted elimination of heavy metal ions with distinct ionic radius [74,75]. This mechanism relies on steric hindrance, where larger ions (*e.g.*, Pb^{2+}, ionic radius 0.119 nm) are sterically excluded from pore entrances, whereas smaller ions (*e.g.*,

Cd^{2+}, 0.097 nm) diffuse freely through the channels. Therefore, the selective removal capacity of different types of POM-based functional materials for different heavy metal ions is closely related to their structural design, surface functional groups, and coordination environment through appropriate modified strategy.

2.4. Recyclability and sustainability

Additionally, POM-based functional materials have good stability under certain conditions, including thermal stability and chemical stability [76–79]. They can maintain a relatively stable structure and performance at higher temperatures, and also retain their basic chemical composition and structure in some organic solvents and aqueous solutions, which makes them have good adaptability under different environmental and application conditions [80–84]. This robustness makes them well-suited for treating extreme wastewater, such as mine drainage and electroplating effluents.

The majority of POM-based functional materials can be regenerated *via* methods such as acid-base treatment, photoreduction, or solvent elution, maintaining excellent performance [85–93]. In terms of green chemistry, employing biological templates like chitosan and cellulose for the synthesis of POM-based functional materials or developing solvent-free/low-solvent synthesis routes, significantly mitigates environmental impacts. These approaches align seamlessly with green chemistry principles, underscoring the sustainability of POM-based functional materials in both production and application.

3. POM-based functional materials for the removal of radionuclides

The remediation of radioactive uranium-laden wastewater represents a formidable global challenge, prompting extensive and systematic research efforts from numerous domestic and international scientific teams [94–99]. In environmental matrices, uranium mainly exists in two oxidation states. Hexavalent U(VI) presents as highly soluble uranyl ions (UO_2^{2+}), which easily migrate through aqueous and soil environments to make separation and enrichment processes more complex. Conversely, tetravalent U(IV) usually forms insoluble compounds, such as uranium dioxide (UO_2) with extremely low solubility in water and much lower migration ability than U(VI). U(IV) precipitates as insoluble UO_2 (solubility product constant, $K_{sp} = -52.0$), conferring enhanced environmental stability [100].

Therefore, the removal and recycling of uranium from nuclear wastewater are of utmost importance for the sustainability of both the environment and nuclear energy. Among these, soluble U(VI) reduced to insoluble U(IV) has emerged as a pivotal strategy. This approach not only mitigates uranium mobility but also offers viable pathways for uranium resource recovery and radioactive pollution control [101–103]. Photocatalytic reduction, a promising method, harnesses the potent reducing power of photogenerated electrons. By continuously supplying electrons to UO_2^{2+}, this process drives the sustained conversion of U(VI) to U(IV), facilitating efficient uranium remediation [104–106]. Consequently, the design and fabrication of high-performance photocatalysts are essential for advancing U(VI) removal efficiency. Among various photocatalytic materials [107], POMs exhibit distinctive features including structural versatility, tunable redox properties, active lattice oxygen sites [108–110], and wide-ranging applications [111–115]. Nevertheless, the exploration of POMs for radioactive wastewater treatment remains in its infancy. An in-depth investigation of their underlying mechanisms and full exploitation of their application potential is imperative for future research.

3.1. Adsorption removal for U(VI)

The surface of POMs is rich in active sites such as terminal oxygen and hydroxyl groups, as well as abundant functional groups (such as phosphate groups, sulfonate groups, carboxyl groups), and carries a negative charge, which can effectively adsorb uranium through coordination or electrostatic attraction. As shown in Fig. 1a, Diwu *et al.* [116] reported that the lacunary Keggin-type POM (PW_9) can selectively bind with U(VI) in the presence of excessive divalent ions, and exhibits an active oxygen scavenging efficiency as high as 78.8 %. The excellent active terminal oxygen quenching ability and uranium removal performance of POMs make them a new type of reagent that can effectively protect the human body from the radiation damage caused by the internal exposure of actinides. Besides the terminal oxygen of [WO_6], the functional groups with a strong affinity for heavy metal ions, such as phosphate and carboxyl, also play a pivotal role in capturing heavy metal ions through coordination interactions or chelation. In Fig. 1b, Xu *et al.* [117] developed a POM-based sorbent $H_{33}Na_{14}Mo^{V}_{24}Mo^{VI}_{2}(PO_4)_{11}O_{73}$ with abundant phosphate groups under hydrothermal conditions, which contains an unprecedented supersodalite cage with an 8.76 Å diameter. As a sorbent, this compound exhibits a maximum sorption capacity of 325.9 mg/g and maintains approximately 90 % of its initial efficiency after five successive sorption/desorption cycles. Then, Liu *et al.* [118] systematically investigated the removal efficiency of POM-based functional materials toward U(VI) by leveraging phosphate groups, which exhibit strong coordination affinity with U(VI). Specifically, the maximum adsorption capacity of CO-POM is 232.04 mg/g under pH 4.0 and 298 K conditions (Fig. 1c).

Nevertheless, pure POMs often face limitations in performance and stability due to agglomeration, disordered molecular arrangements, and restricted specific surface areas [119]. To address these challenges, dispersing POMs within suitable solid matrices has emerged as a viable strategy. MOFs, graphene oxide, and COFs renowned for their porous architectures and chemical robustness, have gained traction as versatile platforms for various applications. Notably, these platforms have demonstrated substantial potential as photocatalysts or adsorbents to remove U(VI) from aqueous systems. Shao *et al.* [120] synthesized a novel POMs ($H_3[\alpha\text{-}PW_{12}O_{40}]$) modified aminated graphene oxide (PHGO). The results show that the maximum adsorption capacity of PHGO for U(VI) is 576 mg/g under conditions of pH 5.0, 298 K, and 6 h. The introduction of POMs could efficiently enhance the interlayer spacing of HGO, meanwhile, the abundant PO_4^{3-} in the POMs structure coordinates with UO_2^{2+}, enhancing the adsorption ability of PHGO for U(VI). In 2016, Ding *et al.* [121] incorporated polyoxometalate $H_3PW_{12}O_{40}$ into the MOFs (HKUST-1@$H_3PW_{12}O_{40}$) and investigated its adsorption performance toward low-concentration U(VI) solutions. The composite material demonstrated selective capture of U(VI) from multi-metal ion mixtures, maintaining stable adsorption capacity even after three desorption-reuse cycles. Structural analysis revealed that abundant carboxyl groups and terminal oxygen moieties in HKUST-1@$H_3PW_{12}O_{40}$ form strong coordination complexes with U(VI) ions, a finding consistent with results from acid-base titration and back titration experiments. In 2024, Yang *et al.* [122] fabricated a high-performance polyoxometalate-based metal-organic framework (POMOF), as illustrated in Fig. 1d, where the abundant oxygen-rich groups of PW_{12} establish strong coordination with uranyl (U(VI)) ions, thereby enabling selective uranium adsorption. Structural and adsorption characterization confirmed that the MIL-101(Cr)@PW_{12} composite achieved an outstanding uranium adsorption capacity of 461.88 mg/g, underscoring the substantial potential of POM-based functional materials for remediating radioactive wastewater. The remarkable adsorption capacity of POM-based functional materials toward

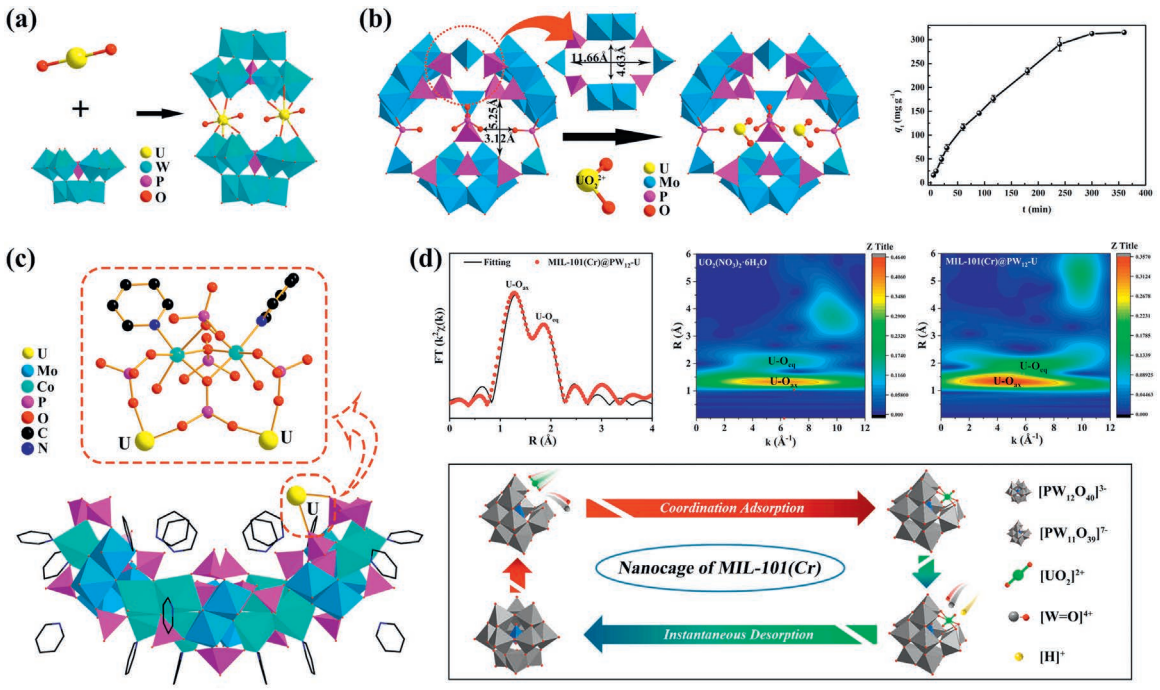


Fig. 1. (a) Complexation mode of PW_9 with uranyl. Reproduced with permission [116]. Copyright 2022, American Chemical Society. (b) Simplified adsorption mechanism of $H_{33}Na_{14}Mo^{V}_{24}Mo^{VI}_{2}(PO_4)_{11}O_{73}$ for uranium. Reproduced with permission [117]. Copyright 2017, American Chemical Society. (c) Schematic illustration of U(VI) adsorption onto CO-POM *via* phosphate groups. Reproduced with permission [118]. Copyright 2019, Elsevier. (d) Experimental EXAFS results, and the adsorption-desorption mechanism of MIL-101(Cr)@PW_{12} for U(VI). Reproduced with permission [122]. Copyright 2024, Elsevier.

U(VI) is primarily attributed to the abundant oxygen-containing functional groups, such as terminal oxo ligands (W=O/Mo=O), phosphate (-PO_4), carboxyl (-COOH) groups. These groups enable efficient chelation of UO_2^{2+} ions through bidentate coordination or electrostatic interaction.

3.2. Synergistic removal mechanism

3.2.1. Synergistic effect of adsorption-photocatalysis reduction

Besides the adsorption capacity, the "electron sponge" property allows POMs to preserve structural integrity during electron gain or loss. This characteristic is capable of effectively facilitating the separation and transfer of photogenerated carriers. Zhang *et al.* dispersed POM (PMo_{12}) in the pores of Cu-MOFs or UiO-66 through a self-assembly strategy to synthesize a series of POM@MOFs (Fig. 2a). Among these, the 15 % PMo_{12}/UiO-66 [123] showed a maximum theoretical adsorption capacity of 225.36 mg/g for U(VI) under dark. Meanwhile, the photocatalytic reduction rate reached 98.92 % under irradiation, approximately 30-fold higher than that of pure UiO-66. During the photocatalytic process, the photogenerated electrons efficiently transfer from UiO-66 to PMo_{12}, which plays a crucial role in the reduction of pre-enriched U(VI) to U(IV). Subsequently, they synthesized POM@Cu-MOFs hybrid materials, demonstrating efficient U(VI) removal through a synergistic effect between adsorption and photocatalysis [124]. In POM, the oxygen-rich moieties serve as adsorption sites, enabling POM@Cu-MOFs to achieve an outstanding removal capacity of 1987.4 mg/g and effectively remove 99.4 % of UO_2^{2+} ions under irradiation. As illustrated in Fig. 2b, Cu-MOFs showcase remarkable adsorption capabilities, whereas POM undergoes reversible multi-electron transfer reactions. These inherent characteristics collectively bestow POM@Cu-MOFs with notable advantages in both adsorption and photocatalytic processes. The generation of free radicals and the underlying reaction mechanisms can be articulated through the following equations:

$$\text{POM@Cu-MOFs} + h\nu \rightarrow e^- + h^+ \quad (1)$$

$$H_2O + h^+ \rightarrow OH + H^+ \quad (2)$$

$$UO_2^{2+} + e^- \rightarrow UO_{2+x}\ (\text{s, amorphism}) \quad (3)$$

$$O_2 + e^- \rightarrow \cdot O_2^- \quad (4)$$

$$UO_2^{2+} + 2O_2^- \rightarrow UO_{2+x}\ (\text{s, amorphism}) + O_2 \quad (5)$$

3.2.2. Synergistic of adsorption-chemical reduction-photocatalytic reduction

Another crucial characteristic of POMs is their remarkable redox property, originating from the variable valence states of the pre-transition metal ions (such as W^{6+}/W^{5+}, Mo^{6+}/Mo^{5+}, V^{5+}/V^{4+}). These valence state changes are often accompanied by the transfer of electrons and the activation of oxygen species, enabling POMs to participate in reactions as electron carriers or redox catalysts. Additionally, the electrons in POMs have delocalization, forming a multi-center redox system, which endows POMs with the relative stability of the overall structure during the process of gaining or losing electrons. In 2024, Qiu *et al.* [125] fabricated a TFHH-POM composite by embedding amino-modified POMs into the pores of highly conjugated polyarylether-based COFs (TFHH) *via* amide bond formation (Fig. 2c). The composite's performance benefits from a trifecta of enhancements: The highly conjugated backbone of TFHH, the charge density disparity between POMs and TFHH, and the spatial confinement of POMs within TFHH pores, all of which act in concert to boost charge separation efficiency. Oxygen-rich groups on POMs and carboxyl moieties on TFHH could selectively bind U(VI) ions, meanwhile, Mo(V) centers in the POMs component efficiently reduce the adsorbed U(VI) to U(IV). Therefore, the U(VI) extraction capacity

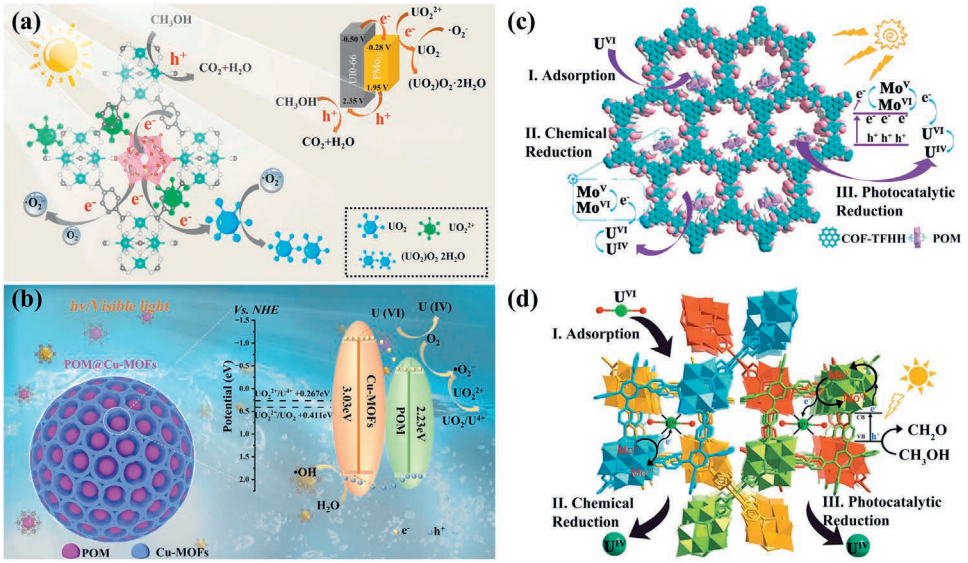


Fig. 2. (a) Synergistic removal mechanism of U(VI) by 15 % PMo_{12}/UiO-66. Reproduced with permission [123]. Copyright 2024, Elsevier. (b) Feasible photoreduction mechanism for U(VI) occurring on the POM@Cu-MOF heterojunction [124]. (c) Synergistic removal mechanism of U(VI) by TFHH-POM. Reproduced with permission [125]. Copyright 2024, Elsevier. (d) Synergistic removal mechanism of U(VI) by [ε-$PMo^{V}_{8}Mo^{VI}_{4}O_{37}(OH)_3Zn_4$]$(TPB)_{3/2}\cdot 6H_2O$. Reproduced with permission [126]. Copyright 2019, Willy Online Library.

of TFHH-POM reaches 489.2 mg/g, thus achieving a synergistic adsorption-chemical reduction-photocatalytic reduction mechanism for uranium removal. In 2019, Wang *et al.* [126] successfully synthesized a POMOFs [ε-$PMo^{V}_{8}Mo^{VI}_{4}O_{37}(OH)_3Zn_4$]$(TPB)_{3/2}\cdot 6H_2O$ (SCU-19) with a triple adsorption mechanism (Fig. 2d). First, U(VI) is adsorbed onto the framework structure of SCU-19 *via* ligand complexation (oxygen atoms). Subsequently, the Mo(V) in the POM unit could chemically reduce the partially adsorbed U(VI) to insoluble U(IV). Under illumination conditions, the photogenerated electrons transfer to the oxidized POMs, thereby forming the reduced POMs that further reduce the additional U(VI) to U(IV) through a photocatalytic reduction process. According to the unique synergy of adsorption-chemical reduction-photocatalytic reduction, the reduction efficiency of POM-based functional materials will be significantly enhanced.

Constructing heterojunctions through the integration of POMs with other semiconductors offers an ingenious and highly efficient approach to the rapid and effective elimination of uranium. This synergistic combination not only leverages the unique redox properties of POMs and the photoactivity of semiconductors but also forms a built-in electric field and achieves the spatial separation of oxidation–reduction, which is another effective way to improve the bulk charge separation efficiency of photocatalytic materials. Liu *et al.* [127] pioneered the fabrication of a novel composite photocatalyst, $(HMTA)_3Pb_2Br_7$@STA-PW_{12}, featuring functionalized POMs encapsulated within perovskite nanotube arrays (Fig. 3a). Capitalizing on the unique "electron sponge" characteristic of POMs, this architecture enables photogenerated electrons efficient transfer from $(HMTA)_3Pb_2Br_7$ to PW_{12}. This rapid electron shuttling mechanism significantly suppresses the photogenerated charge recombination, thereby optimizing charge separation and transport dynamics. Under simulated sunlight irradiation, $(HMTA)_3Pb_2Br_7$@STA-PW_{12} demonstrated extraordinary performance when treating solutions with an initial U(VI) concentration of 40 ppm, achieving an impressive 99.3 % removal of U(VI) within just 40 min (Fig. 3b). In 2024, Li *et al.* [128] were the first to devise a strategy for creating amidoxime-functionalized POM-based porous ionic crystals (PW_{12}AO). Subsequently, they integrated PW_{12}AO with Gd/CdS to fabricate a Z-scheme heterojunction (Fig. 3c). Impressively, the adsorption capacity of Gd/CdS-PW_{12}AO is 205.29 mg/L, and it achieved an outstanding uranium removal efficiency of 90 % in the treatment of solutions with an initial uranium concentration of 300 mg/L without any sacrificial agents. According to the energy band diagram (Fig. 3d), electrons in Gd/CdS will spontaneously migrate to PW_{12}AO to create a built-in electric field oriented from Gd/CdS to PW_{12}AO. Under illumination, both components generate electron-hole pairs and form a Z-scheme heterojunction, which effectively separates charge carriers and maintains a high redox potential, enhancing the composite's photocatalytic performance for uranium removal (Eqs. 6–10).

$$Gd/CdS + hv \rightarrow e^- + h^+ \quad (6)$$

$$PW_{12}AO + hv \rightarrow e^- + h^+ \quad (7)$$

$$UO_2{}^{2+} + 2e^- \rightarrow UO_2 \quad (8)$$

$$O_2 + e^- \rightarrow \cdot O_2{}^- \quad (9)$$

$$H_2O + h^+ \rightarrow \cdot OH + H^+ \quad (10)$$

Besides the photocatalysis and adsorption strategies mentioned above, electrochemical extraction of uranium from seawater holds promise for sustainably supplying nuclear fuel. However, current progress is hindered by the co-deposition of impurities. Zhu *et al.* [129] reported the design of an interfacial coordination-reduction interface in CMOS@NSF, enabling the electrochemical extraction of black UO_2 products from seawater. The internal sulfur in Co-MoOS modulates electron distribution, leading to electron accumulation at terminal O sites for strong binding with uranyl ions. Simultaneously, the interfacial connection between CoMoOS and Ni_3S_2 accelerates electron transfer and enhances reductive properties. This synergistic coordination-reduction interface ensures the formation and stabilization of tetravalent uranium, preventing the co-deposition of alkali metals during crystalline transformation. As illustrated in Figs. 4a-d, when applied to natural seawater, CMOS@NSF demonstrates an electrochemical extraction capacity of 2.65 mg g^{-1} d^{-1}, yielding black UO_2 solid as the final product. Additionally, as a byproduct of nuclear power generation, americium

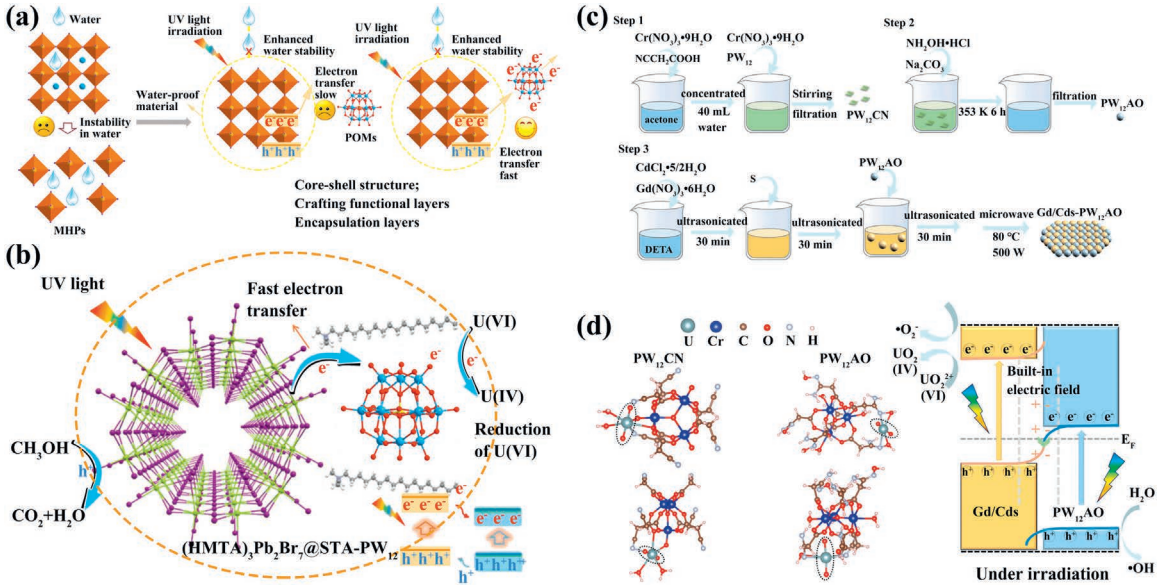


Fig. 3. (a) Stability and carrier transfer capability of $(HMTA)_3Pb_2Br_7$@STA-PW_{12}. (b) Synergistic removal mechanism of U(VI) by $(HMTA)_3Pb_2Br_7$@STA-PW_{12} [127]. (c) Synthesis process of Gd/CdS-PW_{12}AO. (d) Adsorption and photocatalysis mechanisms of PW_{12}CN and PW_{12}AO with U(VI). Reproduced with permission [128]. Copyright 2024, Elsevier.

is a primary source of long-term radiotoxicity in nuclear waste, which poses the greatest environmental hazard after uranium-plutonium separation in nuclear waste.

The separation of americium from lanthanides (Ln) in spent nuclear fuel is crucial for the sustainable development of nuclear energy. According to the coordination chemistry of americium(VI), Wang *et al.* [130] developed a novel inorganic defect POMs cluster $\{Se_6W_{45}\}$, featuring a vacancy site that enables selective coordination of hexavalent actinides (^{238}U, ^{237}Np, ^{242}Pu, and ^{243}Am) over trivalent lanthanides in nitric acid media. The initial $\{Se_6W_{39}\}$ features a macrocyclic architecture with a cavity measuring 8.7 × 8.7 Å. Upon self-assembly, three WO_6^{6-} groups plug the frontal cavity of the POM, while three additional WO_6^{6-} groups cap its rear, generating a vacancy site with a preorganized coplanar oxo-donor framework for precisely matching the actinyl ion. Therefore, $\{Se_6W_{45}\}$ could exhibit an extremely strong complexation with the common pentagonal bipyramid coordination geometry of Am(VI), while showing negligible interaction with trivalent europium (Eu(III)) with spherical configuration. The primary cause of this phenomenon lies in the size differences and coordination mode between lanthanide and actinide species. Additionally, single-crystal X-ray diffraction analysis confirms complete encapsulation of Am(VI) within the designed lacunary binding site, further validating the precise recognition of Am(VI) by the lacunary POM framework (Fig. 4e). Based on this, they developed a new ultrafiltration separation method that holds potential for applications in critical tasks such as spent nuclear fuel reprocessing, radioactive contamination control, separation/purification of radioactive isotopes, and radiochemical diagnostic analysis in China. A comparison of the removal capabilities of some compounds in removing heavy metal ions is illustrated in Table 1.

4. POM-based functional materials for the removal of heavy metal ions

4.1. Catalytic reduction or selective detection for chromium(VI)

In addition to radionuclides, the environmental impact of heavy metal ions (*e.g.*, Cr, Pb, Cd) cannot be overlooked. Among these, chromium is widely employed in industrial production, giving rise to severe environmental challenges [131]. Chromium pollution predominantly stems from wastewater, exhaust gases, and solid wastes discharged by industries such as metal processing, electroplating, and leather manufacturing [132]. The hazard levels of chromium vary significantly across different valence states, with hexavalent chromium (Cr^{6+}) being particularly toxic due to its strong oxidizing properties. Chromium pollution is notoriously difficult to remediate and has a prolonged treatment cycle, posing a grave threat to ecological and environmental security and human health. Therefore, urgent measures are required to strengthen source prevention and control, as well as pollution remediation, to mitigate its environmental risks. Han *et al.* [133] successfully isolated three phosphomolybdate hybrid compounds $(H_2bpp)_2[Fe(H_2O)][Sr(H_2O)_4]_2\{Fe[Mo_6O_{12}(OH)_3(H_2PO_4)(HPO_4)(PO_4)_2]_2\}\cdot 5H_2O$ (**1**), $(H_2bpp)_2[Na(H_2O)(OC_2H_5)][Fe(H_2O)_2][Ca(H_2O)_2]_2\{Fe[Mo_6O_{12}(OH)_3(H_2PO_4)(HPO_4)(PO_4)_2]_2\}\cdot 4H_2O$ (**2**) and $(H_2bpe)_3\{Fe[Mo_6O_{12}(OH)_3(HPO_4)_3(H_2PO_4)]_2\}\cdot 8H_2O$ (**3**). The three hybrids consist of supramolecular networks built up by noncovalent interactions between $\{Fe[P_4Mo_6^{V}O_{31}]_2\}$ polyanions and protonated organic cations. As supramolecular catalysts for the reduction of Cr(VI), organic bpp-containing hybrids **1** and **2** exhibit excellent catalytic activity in the Cr(VI)-formic acid (FA) system at 75 °C, exceeding 95 % of reduction efficiency for Cr(VI) within 180 min (Fig. 5a). However, a single FA exhibits no reducing activity toward Cr(VI). The dominant processes are the physical adsorption of POMs and the surface catalytic reaction between Cr(VI) and FA at low temperatures. When POMs act as a catalyst, it significantly lowers the activation energy to accelerate electron transfer in the Cr(VI)-FA system. With increasing temperature, the reaction mechanism shifts to primarily involve FA reducing POM, with the resulting product then further reducing Cr(VI) to Cr(III) (Eqs. 11 and (12).

$$FA + 2POM \rightarrow 2POM^{-} + CO_2 + 2H^{+} \quad (11)$$

$$6POM^{-} + Cr_2O_7^{2-} + 14H^{+} \rightarrow 6POM + 2Cr^{3+} + 7H_2O \quad (12)$$

Wang *et al.* [134] synthesized three visible-light-responsive Fe-POMs (FePW, FeSiW, and FePMo) by precipitating Fe^{3+} with Keggin-type POMs ($H_3PW_{12}O_{40}$, $H_4SiW_{12}O_{40}$, or $H_3PMo_{12}O_{40}$) (Fig. 5b). Under visible light irradiation, FePMo achieved approximately 88 % reduction of Cr(VI) within 50 min, maintaining good

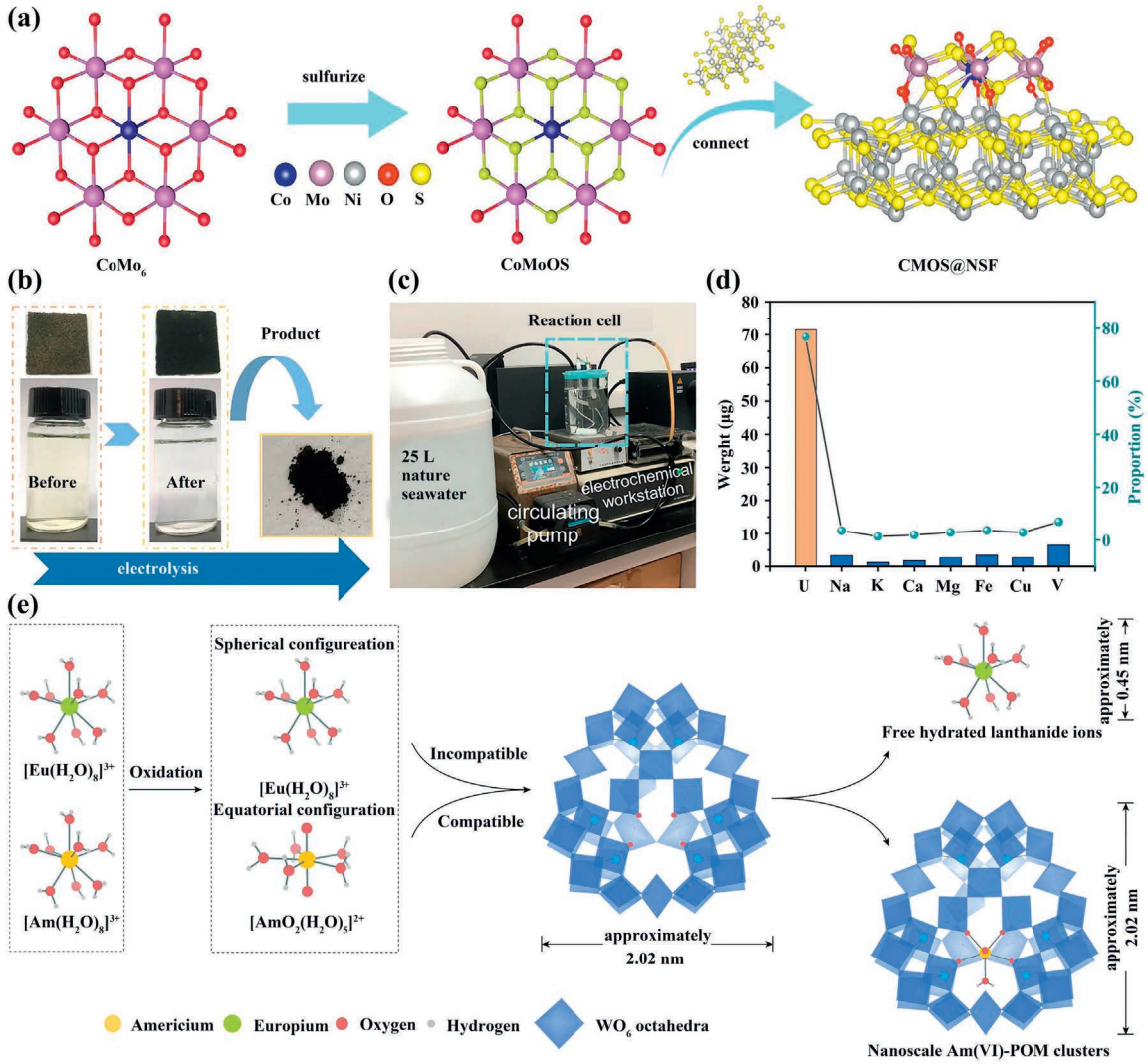


Fig. 4. (a) Synthesis process of COMS@NSF. (b) Photographic records of electrodes and solutions in their pre- and post-reaction states, along with images of the collected products. (c) Self-assembled apparatus designed for the electrochemical extraction of uranium from seawater. (d) Elemental composition analysis of the eluate derived from electrode sheets. Reproduced with permission [129]. Copyright 2025, Springer. (e) Schematic diagram depicting the separation of nanoscale Am(VI)-POM clusters from lanthanide ions. Reproduced with permission [130]. Copyright 2023, Springer.

stability over 5 cycles. The calculated rate constant (0.042 min^{-1}) was 2.5 times and 1.8 times higher than those of FePW and Fe-SiW, respectively. In FePMo, photogenerated electrons in the lowest unoccupied molecular orbital (LUMO) are transferred to Cr(VI), facilitating its reduction. Meanwhile, holes in the highest occupied molecular orbital (HOMO) can directly oxidize organic substances or trigger the formation of reactive $HO^{\bullet}$ radicals.

Based on the above analysis, the potential mechanism of catalytic reduction for Cr(VI) can be attributed to the following aspects. On the one hand, the suitable visible-light response and photoelectrochemical properties are beneficial for the generation, separation, and transfer of electron-hole pairs during the photocatalytic process. The photogenerated electrons in LUMO and the holes in HOMO of POM-based functional materials play a crucial role in Cr(VI) reduction. On the other hand, the excellent oxidation-redox properties of POMs could achieve effective electron transfer through the valence state change, directly reducing Cr(VI) to Cr(III).

Ultra-trace selective detection of heavy metal ions is critically vital in environmental governance and public safety, emerging as a pivotal technical approach to strike a balance between ecological protection and socioeconomic development. A series of POM-based crystalline materials [135–139] have been constructed and applied as an electrochemical sensor for detecting trace Cr(VI), including $[Cu^{I}(BBTZ)]_4[Mn^{II}(H_2O)_3]_2[Cu^{II}(P_4MoV_6O_{31}H_7)_2]\cdot H_3PO_4\cdot 3H_2O$ and $Na^{I}_2(H_2BBTZ)[Na^{I}(H_2O)(BBTZ)]_2[Mn^{II}(H_2O)_2]_2[Mn^{II}(P_4MoV_6O_{31}H_6)_2]\cdot 2H_2O$, $[HC_5H_6N_2]_6\{M[Mo_6O_{12}(OH)_3(HPO_4)_3(H_2PO_4)]_2\}\cdot nH_2O$ (M = Co/Ni/Cd; $n = 2/3$), $(H_2bpp)_2[Na_4Fe(H_2O)_7][Fe(P_4Mo_6O_{31}H_6)_2]\cdot 2H_2O$ and $(H_2bpp)_6(bpp)_2[Fe(P_4Mo_6O_{31}H_8)_2]_2\cdot 13H_2O$, $(H_2L)_2[Co_3(P_4Mo_6O_{31})_2]\cdot 5H_2O$ (**CUST-572**) and $[Mn(P_4Mo_6O_{32})]\cdot 5H_2O$ (**CUST-573**) (Fig. 5c).

The underlying mechanism of the above-mentioned works for the remarkable electrochemical performance is attributed to the synergistic interaction at the molecular level between the reduced $\{P_4Mo_6\}$ clusters and heterometallic centers. $\{P_4Mo_6\}$ clusters coupled with various heterometallic centers (Cu(I), Cu(II), Mn(II), Fe(III)), which achieve efficient electrochemical detection of ultra-trace Cr(VI) accompanied by excellent anti-interference capability and electrochemical stability. In addition to the synergistic interaction between $\{P_4Mo_6\}$ clus-

Table 1
Efficiency comparison of some compounds in removing heavy metal ions.

Compounds	Removal of heavy metals	Removal capacity/removal rate	Strategy	Active sites	Ref.
CO-POM	U(VI)	232.04 mg/g	Adsorption	PO_4^{3-}	[118]
POM-HGO	U(VI)	576 mg/g	Adsorption	–COOH, $–NH_2$, PO_4^{3-}	[120]
HKUST-1@$H_3PW_{12}O_{40}$	U(VI)	14.58 mg/g	Adsorption	-COOH,	[121]
MIL-101(Cr)@PW_{12}	U(VI)	461.88 mg/g	Adsorption	Oxygen groups, pore structure,	[122]
PMo_{12}/UiO-66	U(VI)	225.36 mg/g	Adsorption and photocatalysis	Terminal O, e^-	[123]
POM@Cu-MOFs	U(VI)	1987.4 mg/g with 99.4 %	Photocatalysis reduction	Terminal O, e^-	[124]
TFHH-POM	U(VI)	289.0 mg/g under dark 489.2 mg/g under illumination	Adsorption-chemical reduction-photocatalytic reduction	Oxygen-containing groups, -COOH, Mo(V)	[125]
[ε-$PMo^{V}_{8}Mo^{VI}_{4}O_{37}(OH)_3Zn_4$]-$(TPB)_{3/2}\cdot 6H_2O$	U(VI)	557.56 mg/g under dark, 728.34 mg/g under illumination	Adsorption-chemical reduction-photocatalytic reduction	Mo(V), e^-	[126]
$(HMTA)_3Pb_2Br_7$@STA-PW_{12}	U(VI)	99.3 %	Photocatalysis reduction	e^-	[127]
Gd/CdS-PW_{12}AO	U(VI)	205.29 mg/L with 90 %	Adsorption and photocatalysis	$[Cr_3O(OOCCH_2CN)_6(H_2O)_3]^+$, $[Cr_3O(OOCCH_2CN_2OH_3)_6(H_2O)_3]^+$, N-O, e^-	[128]
CMOS@NSF	U(VI)	2.65 mg g^{-1} d^{-1}	Electrochemical reduction	Terminal O, e^-	[129]
$H[Cu^{I}(Hbcbpy)_4(PW_{12}O_{40})_2]\cdot 7H_2O$	Cr(VI)	91.94 %	Photocatalytic reduction	e^-	[71]
$\{Fe[P_4Mo_6VO_{31}]_2\}_2$ polyanions	Cr(VI)	95 %	Catalytic reduction	HCOOH, POM^-	[133]
FePMo	Cr(VI)	88 %	Photocatalytic reduction	Oxidative HO• radicals	[134]
LPOM@ZIF	Pb^{2+}	764 mg/g	Adsorption	Vacant oxygen sites, -NH	[140]
HKUST-1-@$H_3PW_{12}O_{40}$	Pb^{2+}, Cd^{2+}, Cr^{3+}	98.18, 32.45, 38.25 mg/g	Adsorption	Pore structure, oxygen-containing groups	[141]
POM@MOFs	Pb^{2+}	772.23 mg/g	Adsorption	Pore structure, N and O atoms	[147]
$(C_5NH_5)_4(C_3N_2H_5)_2Zn_3(H_8P_4Mo_6O_{31})_2\cdot 2H_2O$	Pb^{2+}	714.7 mg/g	Adsorption	PO_4^{3-}	[128]
$PW_{10}Mo_2$-SBA-15	Co^{2+}, Sr^{2+}	87.72 mg/g for Co^{2+} 80.01 mg/g for Sr^{2+}	Adsorption	Oxygen-containing groups, $-NH_2$	[149]
PONb nanoclusters (FZU-1)	Sr^{2+}	62.8 mg/g	Adsorption	Concavity site, oxygen-containing groups,	[150]
$Q^{10}[Mo_{46}]$@SiO_2@Fe_3O_4 $Q^8[Mo_{54}]$@SiO_2@Fe_3O_4 $Q^8[Mo_{46}]$@SiO_2@Fe_3O_4 $Q^{10}[Mo_{54}]$@SiO_2@Fe_3O_4	Pb^{2+}, Cu^{2+}, Co^{2+}, Ni^{2+}, Hg^{2+}, Cd^{2+}	79.5 % to 99.3 % in laboratory water 92 % to 99 % in industrial wastewater	Adsorption	Large specific surface, oxygen-containing groups	[151]
$Q^8[Mo_{64}Ni_8La_6]$@SiO_2@Fe_3O_4 $Q^{10}[Mo_{176}/Mo_{248}]$@$SiO_2$@$Fe_3O_4$ $Q^8[Mo_{176}/Mo_{248}]$@SiO_2@Fe_3O_4 $Q^{10}[Mo_{64}Ni_8La_6]$@SiO_2@Fe_3O_4	Pb^{2+}, Cu^{2+}, Co^{2+}, Ni^{2+}, Hg^{2+}, Cd^{2+}	87.35 % to 99.98 %	Adsorption	Large specific surface, oxygen-containing groups	[152]
$[H_n(\gamma\text{-}SiW_{10}O_{32})_2(\mu\text{-}O)_4]^{(8-n)-}$	Pb^{2+}, Sr^{2+}, Ag^+, Na^+, K^+, Rb^+	/	Encapsulation	A rigid cavity	[153]
NH_4-PMo	Ni^{2+}	34.8 mg/g	Adsorption	Negative surface charges and higher specific surface area	[154]
PMo_{12}/ZIF-8	Cs^+	291.5 mg/g	Adsorption	Negative charge, pore structure	[157]
[α-$PMo^{VI}_{12}O_{40}$]$^{3-}$@[$Mo^{VI}_{72}Fe^{III}_{30}O_{252}(H_2O)_{102}(CH_3CO_2)_{15}$]$^{3+}$ $\cdot 60H_2O$	Cs^+	83 mg/g	Adsorption	Cation-coupled electron-transfer	[158]
$(etpyH)_2[Cr_3O(OOCH)_6(etpy)_3]_2$[a-$SiMo_{12}O_{40}$]$\cdot 3H_2O$ (etpy = 4-ethylpyridine)	Cs^+	3.5 mol(Cs^+)mol(s)$^{-1}$	Reduction-induced ion exchange method	Pore structure, cation exchange	[159]

ters and heterometallic centers, the construction of POM-based metal-organic complexes (MOCs) is another excellent electrochemical sensor to detect Cr(VI). As shown in Fig. 5d, two novel POM-based MOCs, $H_3[Cu_2(4\text{-dpye})_2(PMo_{12}O_{40})]$ (**1**) and $H[Cu_2(4\text{-Hdpye})_2(PMo_{12}O_{40})(H_2O)_4]\cdot 2H_2O$ (**2**) (4-H_2dpye = *N*,*N*'-bis(4-pyrimidinecarboxamido)-1,2-ethane) [140] were constructed and used as electrochemical sensors, the detection limits achieved were as low as 1.27×10^{-7} mol/L for 1-CPE and 1.71×10^{-7} mol/L for 2-CPE. Based on the above analysis, a comparison of the detection limits for specific compounds used in the detection of heavy metal ions is presented in Table 2.

4.2. Adsorption removal for lead(II)

Among the heavy metal ions, lead (Pb(II)) with strong toxicity and high bioaccumulation potential poses multi-dimensional threats to aquatic ecosystems and human health. Thus, developing efficient and reliable strategies for Pb(II) remediation is vitally important and urgent. As illustrated in Fig. 6a, Chen *et al.* [141] reported a self-assembly method to encapsulate lacunary POMs (LPOMs) within tailored cavities of zeolitic imidazolate frameworks (ZIFs), yielding LPOM@ZIF. By tuning vacant oxygen sites, LPOM@ZIF achieves 764 mg/g of capture capacity. In which

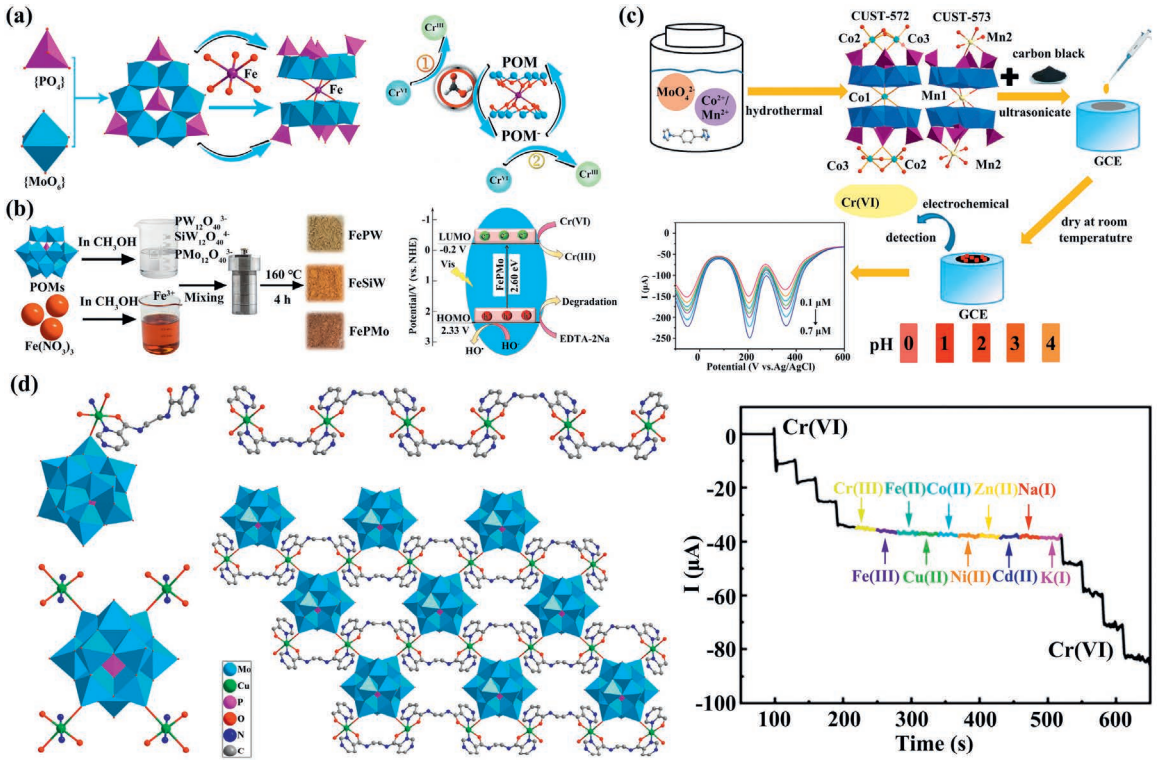


Fig. 5. (a) The assembly process of $\{Fe(P_4Mo_6O_{31})_2\}$, and the proposed mechanism for reduction of Cr(VI) [133]. (b) Preparation processes for different Fe-POMs and the proposed charge transfer mechanism [134]. (c) Synthesis of $\{Co_3(P_4Mo_6O_{31})_2\}$(CUST-572) and $\{Mn(P_4Mo_6O_{32})_2\}$(CUST-573) and trace determination for Cr(VI). Reproduced with permission [139]. Copyright 2023, Elsevier. (d) Structure of $H_3[Cu_2(4\text{-dpye})_2(PMo_{12}O_{40})]$ and the current response changing with different metal ions [140].

Table 2
Comparison of detection limits for some compounds in detecting heavy metal ions.

Compounds	Detection of heavy metals	Limits of detection	Ref.
$[Cu^{I}(BBTZ)]_4[Mn^{II}(H_2O)_3]_2[Cu^{II}(P_4MoV_6O_{31}H_7)_2]\cdot H_3PO_4\cdot 3H_2O$ (**1**)	Cr(VI)	1.59 nmol/L for **1**	[135]
$Na^{I}_2(H_2BBTZ)[Na^{I}(H_2O)(BBTZ)]_2[Mn^{II}(H_2O)_2]_2[Mn^{II}(P_4MoV_6O_{31}H_6)_2]\cdot 2H_2O$ (**2**)		2.91 nmol/L for **2**	
$(H_2bpp)_2[Na_4Fe(H_2O)_7][Fe(P_4Mo_6O_{31}H_6)_2]\cdot 2H_2O$ (**1**)	Cr(VI)	0.79 μmol/L for **1**	[136]
$(H_2bpp)_6(bpp)_2[Fe(P_4Mo_6O31H8)_2]_2\cdot 13H_2O$ (**2**)		0.33 μmol/L for **2**	
$[HC_5H_6N_2]_6\{M[Mo_6O_12(OH)_3(HPO_4)_3(H_2PO_4)]_2\}\cdot nH_2O$	Cr(VI)	0.026 μmol/L (0.0027 ppm)	[137]
$(H_2bib)_2[Cd(H_2O)]_2[Na(H_2O)_{0.5}][Cd(P_4Mo_6O_{31}H_{6.5})_2]\cdot 13H_2O$ (**1**)	Cr(VI)	18.41 nmol/L for **1**	[138]
$(H_2bib)_2[Cd(bib)(H_2O)]_2[Cd(P_4Mo_6O_{31}H_7)_2]\cdot 17H_2O$ (**2**),		30.86 nmol/L for **2**	
$(H_2bib)_2Cd[Cd(P_4Mo_6O_{31}H_8)_2]\cdot 13H_2O$ (**3**) (bib = 4,4′-bis(imidazolyl)biphenyl)		38.90 nmol/L for **3**	
$(H_2L)_2[Co_3(P_4Mo_6O_{31})_2]\cdot 5H_2O$ (**CUST-572**)	Cr(VI)	133.89 μA L/μmol and 30.05 μA L/μmol	[139]
$[Mn(P_4Mo_6O_{32})]\cdot 5H_2O$ (**CUST-573**)			
$H_3[Cu_2(4\text{-dpye})_2(PMo_{12}O_{40})]$ (**1**)	Cr(VI)	1.27×10^{-7} mol/L for **1**	[140]
$H[Cu_2(4\text{-Hdpye})_2(PMo_{12}O_{40})(H_2O)_4]\cdot 2H_2O$ (**2**)		1.71×10^{-7} mol/L for **2**	
$Na_9[BiW_9O_{33}]\cdot 16H_2O$	Cd(II), Pb(II)	9.9 nmol/L for Cd(II) and 14.2 nmol/L for Pb(II)	[143]
$H_3PW_{12}O_{40}\cdot H_2O$	Pb^{2+}, Cd^{2+}	1×10^{-8} mol/L and 2×10^{-7} mol/L	[144]

$PW_{11}O_{39}$@ZIF-8 maintained excellent removal efficiency (~98.5 %) for Pb(II) from the mixture solution containing competing ions. Meanwhile, LPOM@ZIF enables ultradeep water purification, reducing Pb(II) concentration from 71,770 ppb to 1.84 ppb within 15 min. Density functional theory (DFT) calculations and experimental results confirmed that oxygen sites in LPOMs contribute to the remarkable Pb(II) adsorption efficiency, while amino groups (ANH) on ZIFs serve as additional adsorption sites. Li *et al.* [142] synthesized HKUST-1@$H_3PW_{12}O_{40}$ *via* a microwave-assisted method. As a highly selective adsorbent material, HKUST-1@$H_3PW_{12}O_{40}$ exhibits excellent adsorption capacity of 98.18 mg/g for Pb^{2+}, 32.45 mg/g for Cd^{2+}, and 38.25 mg/g for Cr^{3+}.

Likewise, electrochemical stripping analysis has been recognized as an effective method for the quantification of heavy metal ions, particularly when applied to bismuth-based materials. Liu *et al.* [143] synthesized $Na_9[BiW_9O_{33}]\cdot 16H_2O$ (abbreviated as BiW_9) and employed it to fabricate an electrochemical sensor for the concurrent detection of Cd(II) and Pb(II) in the concentration range of 1–50 μmol/L. The detection limits of Cd(II) and Pb(II) were 9.9 and 14.2 nmol/L, respectively. Kang *et al.* [144] demonstrated that well-defined colloidal carbon nanospheres (CNSs) could be synthesized on a large scale with the assistance of POMs, along with 1×10^{-8} and 2×10^{-7} mol/L of the detection limits for Pb(II) and Cd(II). Thus, the electrochemical sensor developed using POM-based functional materials demonstrates excellent performance for the detection of heavy metal ions, holding promise for further practical applications in real-world scenarios.

Another important source of lead pollution is emerging perovskite solar cells (PSCs). Lead-based PSCs have emerged as the most promising candidates for next-generation photovoltaic devices for commercialization due to the advantages of simple preparation processes, low cost, and excellent optoelectronic proper-

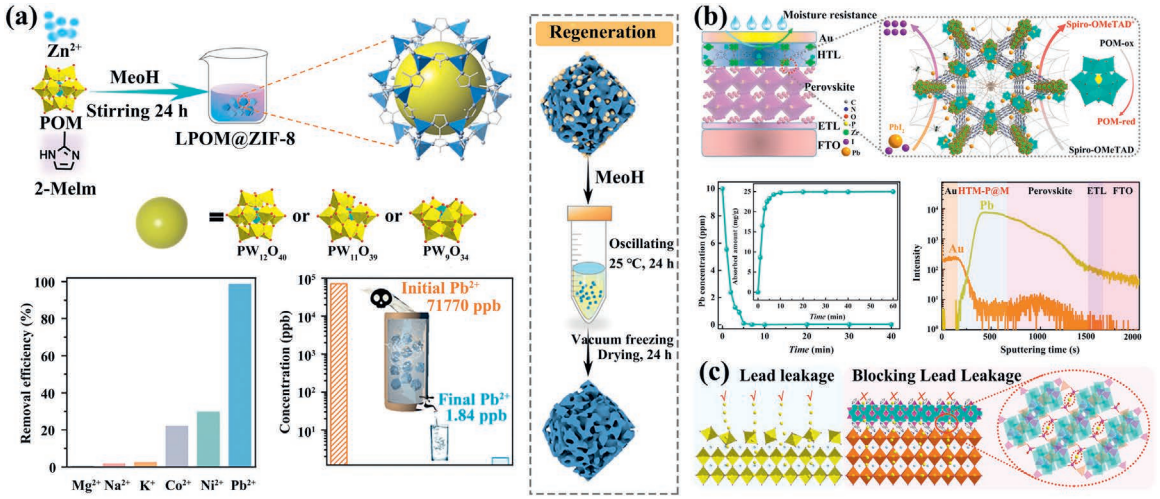


Fig. 6. (a) Preparation of LPOM@ZIF-8, and the selective adsorption for Pb(II). Reproduced with permission [141]. Copyright 2021, Elsevier. (b) Schematic of the effects of POM@MOFs on suppressing lead leakage. Reproduced with permission [148]. Copyright 2022, Elsevier. (c) The suppression schematic of lead leakage by POMOF. Reproduced with permission [149]. Copyright 2023, Willy Online Library.

ties [145]. However, the highly toxic heavy metal lead remains the primary component of the light-absorbing layer in high-efficiency PSCs [146,147]. Therefore, the toxicity and leakage of heavy metal lead from perovskite films pose serious environmental safety risks, serving as one of the key obstacles limiting the eco-friendly development of PSCs. Aiming at the toxicity and leakage issues of Pb(II), Yang *et al.* [148] developed a series of POM@MOFs host-guest nanostructured dopants (Fig. 6b). Notably, the maximum uptake capacity of POM@MOFs for Pb(II) reached 772.23 mg/g, and POM@MOFs captured over 70 % of Pb(II) leaked from degraded PSCs, which was further validated by time-of-flight secondary-ion mass spectrometry (TOF-SIMS). The large number of active sites, such as N atoms in the porphyrin ring and terminal O atoms of POMs, plays a crucial role in the adsorption of Pb(II). In 2023, a novel two-dimensional POMOF $(C_5NH_5)_4(C_3N_2H_5)_2Zn_3(H_8P_4Mo_6O_{31})_2{\cdot}2H_2O$ was constructed to address lead leakage and stability challenges (Fig. 6c) [149]. The above results showed that POM-based functional materials, featuring abundant active groups (such as PO_4^{3-}, oxygen-containing groups, and N atoms) and pore structure, exhibit both *in situ* chemical anchoring and adsorption capabilities for toxic lead ions through well-defined chemical interactions, thereby reducing environmental risks.

4.3. Simultaneous removal of other heavy metals

Industrial or laboratory wastewater often contains various heavy metal ions, such as cobalt (Co^{2+}) and strontium (Sr^{2+}), cadmium (Cd^{2+}), copper (Cu^{2+}), nickel (Ni^{2+}), silver (Ag^{+}), mercury (Hg^{2+}), and arsenic (As^{3+}/As^{5+}). These heavy metal ions pose serious threats to ecological environments and human health. Therefore, effective treatment of these heavy metal ions in industrial wastewater through simple methods or multi-functional materials is crucial for environmental protection and sustainable development. As shown in Fig. 7a, Mahjoub *et al.* [150] prepared amine-functionalized magnetic SBA-15 to support 10-tungsten-2-molybdophosphoric acid ($H_3[PMo_2W_{10}O_{40}]{\cdot}nH_2O$), and utilized this material as an efficient inorganic adsorbent for the simultaneous removal of Co^{2+} and Sr^{2+}. The adsorption capacity is 87.72 mg/g for Co^{2+} and 80.01 mg/g for Sr^{2+}. Additionally, Zheng *et al.* [151] proposed a site differentiation strategy and constructed the giant polyoxoniobate (PONb) nanoclusters of an all-inorganic PONb framework (FZU-1). This configuration results in a total of 12 such concavity sites on each Dy12Nb84, which is suitable for the recognition and selective capture of Sr^{2+} ions due to the appropriate Sr-O bond lengths. Therefore, FZU-1 could effectively remove 98.9 % of Sr^{2+} from simulated nuclear liquid waste due to the presence of distinct selective metal capture sites (concavity site and tweezer site). In Fig. 7b, Sohail *et al.* [152,153] reported a series of POM-based ionic liquids reinforced on magnetic nanoparticles, including $Q^8[Mo_{54}]@SiO_2@Fe_3O_4$, $Q^{10}[Mo_{54}]@SiO_2@Fe_3O_4$, $Q^8[Mo_{46}]@SiO_2@Fe_3O_4$, $Q^{10}[Mo_{46}]@SiO_2@Fe_3O_4$ (Q denotes long-chain alkyl quaternary ammonium salts, where Q^{10} is tetraoctylammonium bromide (TOA-Br) and Q^{10} is tetrakis(decyl)ammonium bromide (TDA-Br)). These materials exhibited remarkable removal efficiencies for Pb^{2+}, Cu^{2+}, Co^{2+}, Ni^{2+}, Hg^{2+}, Cd^{2+}, ranging from 79.5 % to 99.3 % in laboratory water and 92 % to 99 % in industrial wastewater. Similarly, another set of materials, $Q^8[Mo_{64}Ni_8La_6]@SiO_2@Fe_3O_4$, $Q^{10}[Mo_{64}Ni_8La_6]@SiO_2@Fe_3O_4$, $Q^8[Mo_{176}/Mo_{248}]@SiO_2@Fe_3O_4$, and $Q^{10}[Mo_{176}/Mo_{248}]@SiO_2@Fe_3O_4$ achieved removal efficiencies for the same ions in the range of 87.35 % to 99.98 %. Those material's exceptional removal efficiency is attributed to the enhanced hydrophobicity of POM-IL-MNPs, which originates from the integration of large molybdenum-based POM clusters with long-chain quaternary organo-ammonium cations (*e.g.*, tetraoctylammonium (TOA) and tetrakis(decyl)ammonium (TDA)). Furthermore, the composite's amorphous surface structure, high specific surface area, and efficient adsorption capabilities collectively drive this outstanding performance.

Constructing multifunctional POM-based functional materials for the simultaneous removal of multiple heavy metal ions holds substantial research significance and practical application value in the field of environmental governance. In Fig. 7c, Streb *et al.* [154] developed a unique multifunctional POM-ionic liquid (POM-IL) immobilized on porous silica for the removal of multiple heavy metals, with each component targeting specific types of water contaminants. POM-IL consists of antimicrobial alkylammonium cations and lacunary POMs anions, which feature heavy-metal binding sites. Ni^{2+}, Pb^{2+}, Cu^{2+}, Cr^{3+}, Co^{2+}, and UO_2^{2+} could be successfully eliminated from water sources through the synergistic action of the POM-SILP, paving the way for multifunctional materials in pollutant adsorption and water purification. Moreover, Ag^{+}, Ni^{2+}, Cd^{2+}, and Cs^{+}, as representative heavy metal ions, pose substantial risks to ecological systems and human health [155–159]. In 2024, Wang *et al.* [160] synthesized a novel POM/viologen-

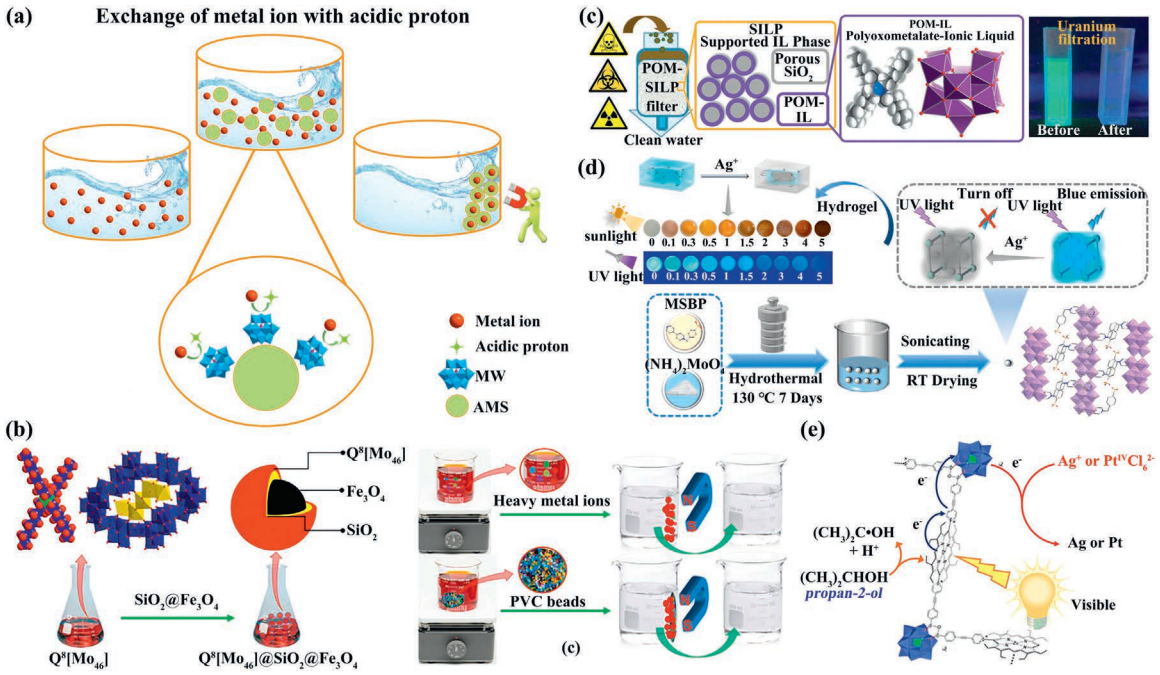


Fig. 7. (a) Adsorption of Co^{2+} and Sr^{2+} ions by $H_3[PMo_2W_{10}O_{40}]\cdot nH_2O$ supported SBA–15. Reprinted with permission [150]. Copyright 2019, the Authors. (b) Synthesis of various compounds and the adsorption process of heavy metal ions. Reproduced with permission [152]. Copyright 2021, Elsevier. (c) Water purification using POM-SILPs. Reproduced with permission [154]. Copyright 2024, Elsevier. (d) Preparation of $[(HMSBP)_2(\gamma\text{-}Mo_8O_{26})]\cdot 4H_2O$ for detecting Ag^+. Reproduced with permission [160]. Copyright 2024, Elsevier. (e) Electron transfer in the case of the photocatalysis of the reduction of Ag(I) or Pt(IV) with propan-2-ol. Reproduced with permission [162]. Copyright 2025, American Chemical Society.

based supramolecular compound, $[(HMSBP)_2(\gamma\text{-}Mo_8O_{26})]\cdot 4H_2O$ (MSBP = 1-(4-methanesulfonylbenzyl)-[4,4′]bipyridinyl-1-ium). The coordination reaction between the S = O groups, pyridine N atoms, and Ag^+ enables the detection of Ag^+, with a detection limit of 0.0411 μmol/L within the concentration range of 0.1–3 μmol/L. Moreover, this supramolecular fluorescent probe has successfully enabled the quantitative monitoring of Ag^+ concentration in environmental water samples and commercially available disinfectant sprays (Fig. 7d).

From an environmental governance perspective, recycling heavy metal ions helps mitigate their harm to the ecological environment [161]. Economically, recycling not only reduces raw material costs in industrial sectors but also drives the development of a waste recycling and reuse industrial chain, achieving the dual benefits of pollution control and resource value added. Therefore, recycling heavy metal ions is an activity that is conducive to the sustainable development of society, which is equally important for environmental governance with effective removal. In 2025, Ruhlmann *et al.* [162] constructed four distinct POM-porphyrin polymers by combining $[PW_{11}Si_2O_{40}C_{26}H_{16}N_2]^{3-}$ or $[P_2W_{17}Si_2O_{62}C_{26}H_{16}N_2]^{6-}$ anions bearing pyridyl units with zinc(II) 2,3,7,8,12,13,17,18-octaethylporphyrin and 5,15-(di-*p*-tolyl)porphyrin (Fig. 7e). The POM subunit, acting as an electron acceptor, exhibits distinct reduction redox potentials depending on its Keggin or Dawson structural type. The Soret and Q bands of the porphyrin subunit dominate the light absorption properties of the POM-porphyrin copolymers. These materials maintained comparable efficiency in the visible-light-driven photoreduction of Pt(IV) without causing any surface poisoning on the catalyst.

5. Conclusion and perspectives

In conclusion, POM-based functional materials have emerged as promising candidates for heavy metal ion remediation and environmental purification, owing to their tunable structural features and exceptional physicochemical properties. This review systematically presents the latest advancements in POM-based functional materials, highlighting their applications in sustainable strategies for heavy metal pollution remediation. At the molecular level, POMs can be precisely engineered by constructing functional materials such as host-guest systems, heterojunctions, and POM-based MOFs, enabling the customization of material properties to target specific heavy metal ions (U(VI), Cr(VI), Cd(II), Sr(II), Ni(II), and Pb(II)).

Based on the above comprehensive analysis, the removal mechanisms towards different kinds of heavy metals exhibit significant divergence, which is mainly ascribed to their intrinsic characteristics and environmental factors that dictate the most effective removal strategies. For radioactive nuclide uranium, U(VI) exists predominantly as highly soluble uranyl ions (UO_2^{2+}), exhibiting strong migration capability in aqueous environments. UO_2^{2+} has a strong tendency to form stable complexes with ligands containing O and N donor atoms. As a result, the removal of U(VI) often relies on materials with functional groups capable of chelating the uranyl ion, such as phosphonic acid groups or amidoxime groups. These functional groups can form multi-dentate complexes with U(VI), ensuring high-affinity binding through chemical adsorption. Meanwhile, soluble U(VI) reduced to insoluble U(IV) has emerged as another pivotal strategy, which utilizes the photogenerated electrons or oxidants to achieve the reduction process through chemical reduction, photocatalytic reduction, or their synergistic removal mechanism.

In contrast, Cr(VI) is highly oxidizing and exists as anionic species (CrO_4^{2-} or $Cr_2O_7^{2-}$) depending on the pH. Its removal typically involves a two-step process. First, catalytic reduction of Cr(VI) to less toxic Cr(III) using reducing agents, followed by precipitation or adsorption. Second, the removal of Cr(III) can be achieved through ion-exchange or chemical complexation with hydroxide-based materials. Additionally, a series of POM-based crystalline materials have been constructed and applied as an electrochemical sensor for detecting trace Cr(VI). For Pb(II), Cd(II), and Cs(I) without variable valence *via* mechanisms such as adsorption, ion-



Fig. 8. The perspectives of POM-based functional materials.

exchange, and precipitation. The negatively charged functional groups (carboxylates, phosphates, sulfonates) in materials can effectively attract and bind those heavy metal ions through chemical bonds or electrostatic interactions. Additionally, the formation of insoluble compounds provides an alternative pathway for the removal of those heavy metal ions.

Despite these significant achievements, current research on POM-based functional materials for heavy metal remediation still faces numerous challenges. One of the major hurdles is large-scale synthesis. Complex and costly techniques are difficult to translate into large-scale production, which limits their widespread application in real-world environmental remediation projects. Another challenge is the long-term stability and recyclability of these materials. POM-based functional materials may suffer from structural degradation, leaching of active components, or fouling by organic matter and other contaminants, reducing their recyclability. Selectivity is also a critical issue, as real environmental samples often contain a complex mixture of heavy metal ions and other interfering substances. Therefore, designing POM-based functional materials with excellent durability and high selectivity towards specific heavy metals is essential for their sustainable use.

To overcome these challenges, the potential research directions and development trends in the future should be focused on the following aspects (Fig. 8).

(1) Structure and performance optimization of POM-based functional materials: It is essential to further develop novel POM-based functional materials featuring ultra-high adsorption capacity and selectivity through rational design and precise construction. Machine learning (ML) and other artificial intelligence (AI) technologies can be utilized to establish systems for data mining, synthesis pathway prediction, reaction condition optimization, structure-property relationship modeling, and automated synthesis system development. This approach enables the design of novel POM structures and the introduction of specific recognition groups, thereby achieving the selective adsorption of specific heavy metal ions.

(2) Mechanism research: Advanced characterization techniques will be employed to further explore the adsorption mechanisms between POM-based functional materials and heavy metal ions. Elucidating specific mechanisms such as chemical bond formation, electron transfer, and ion exchange can provide a robust theoretical basis for material design and optimization. Simultaneously, the dynamic processes of heavy metal ion adsorption by POM-based functional materials, including adsorption kinetics and thermodynamics warrant further investigation.

(3) Expansion of practical applications: In future research, efforts can be concentrated on developing large-scale synthesis methods for POM-based functional materials and enhancing application research in areas such as advanced industrial wastewater treatment, drinking water safety assurance, and *in situ* soil and water remediation. Concurrently, a technical system of "adsorption-recycling-regeneration" will be established to realize the coordinated development of resource recycling and environmental protection.

(4) Green synthesis and sustainable development: Green approaches such as biosynthesis, microwave-assisted synthesis, and mechanochemical synthesis will be adopted to develop eco-friendly and low-cost synthesis technologies for POM-based functional materials. Additionally, a full life cycle assessment system for materials will be established to comprehensively evaluate their environmental impacts and economic benefits across the entire chain, from synthesis and application to recycling, thereby promoting the sustainable development of this field.

Declaration of competing interest

The authors declare that they have no known competing financial interests or personal relationships that could have appeared to influence the work reported in this paper.

CRediT authorship contribution statement

Yayu Dong: Writing – review & editing, Writing – original draft, Methodology, Data curation, Conceptualization. **Jinghan Hao:** Software, Data curation. **Yingcai Wang:** Writing – review & editing, Data curation. **Xiaohong Cao:** Writing – review & editing, Data curation. **Zhimin Dong:** Writing – review & editing, Writing – original draft, Project administration, Funding acquisition, Data curation, Conceptualization. **Zhibin Zhang:** Writing – review & editing, Writing – original draft, Project administration, Funding acquisition. **Yunhai Liu:** Writing – review & editing, Writing – original draft, Project administration, Funding acquisition.

Acknowledgments

This work was financially supported by the National Natural Science Foundation of China (Nos. 22466005, 22276030, 22376025). Natural Science Foundation of Jiangxi Province (Nos. 20232BAB213034, 20232ACB203011). Young Elite Scientists Sponsorship Program by JXAST (No. 2025QT08). The start-up funds of East China JiaoTong University (No. 2003424011).

References

[1] B. He, Z. Yun, J. Shi, et al., Chin. Sci. Bull. 58 (2013) 134–140.
[2] B.R. Shetty, P.B. Jagadeesha, S.A. Salmataj, CyTA-J Food. 23 (2025) 2438726.
[3] S.L. Wang, M.R. Razanajatovo, X.D. Du, et al., Chin. Chem. Lett. 35 (2024) 109140.
[4] S. Rajendran, T.A.K. Priya, K.S. Khoo, et al., Chemosphere 287 (2022) 132369.
[5] A. Chatterjee, J. Abraham, Biotechnol. Lett. 41 (2019) 319–333.
[6] X.R. Mai, J. Tang, J.X. Tang, et al., J. Environ. Sci. 149 (2025) 1–20.
[7] J.P. Vareda, A.J.M. Valente, L. Duraes, J. Environ. Manage. 246 (2019) 101–118.
[8] Y. Xie, Z. Liu, H.Y. Geng, et al., Chem. Soc. Rev. 52 (2023) 97–162.
[9] Z.T. Zeng, S.Y. Fang, D.T. Tang, et al., Microporous Mesoporous Mater. 284 (2019) 177–185.
[10] H. Liu, B.Y. Xiao, Y.M. Zhao, et al., Chin. Chem. Lett. 36 (2025) 110619.
[11] Q. Lan, S.J. Jin, Y. Liu, X.L. Jin, et al., Tungsten 7 (2025) 243–254.
[12] G. Murtaza, M.I. Ahmed, K. Yu, et al., Environ. Res. 272 (2025) 121156.
[13] J. Yang, Z. Yi, J. Li, et al., Nat. Commun. 16 (2025) 2922.
[14] C. Li, W. Liu, X. Chen, et al., Chin. Chem. Lett. 35 (2024) 109652.
[15] M. Aarthy, T. Rajesh, M. Thirunavoukkarasu, J. Chem. Technol. Biotechnol. 95 (2020) 1298–1307.
[16] J.Z. Ma, M.Z. Xia, S.D. Zhu, et al., J. Hazard. Mater. 400 (2020) 123143.

[17] J.H. Qu, Y.H. Yuan, Q.J. Meng, et al., J. Hazard. Mater. 400 (2020) 123142.
[18] J.L. Zhao, C. Wang, S.X. Wang, et al., J. Ind. Eng. Chem. 83 (2020) 111–122.
[19] H. Li, Q.L. Zhao, H. Zhang, et al., Sep. Purif. Technol. 367 (2025) 132968.
[20] Z. Wang, J.B. Lu, X. Dong, et al., J. Am. Chem. Soc. 144 (2022) 6383–6389.
[21] Z.M. Dong, D.L. Gao, Z.F. Li, et al., Energy Environ. Mater. 7 (2024) e12705.
[22] Y.T. Wu, P.J. Li, L. Chen, et al., ACS Sustain. Chem. Eng. 12 (2024) 6659–6665.
[23] W.L. Bao, T. Yu, Y.N. Liu, et al., Coord. Chem. Rev. 539 (2025) 216748.
[24] H. Liu, Q. Yang, N. Luan, et al., Nat. Sustain. 8 (2025) 553–561.
[25] Y. Duan, Y. Sun, A. Palomo, et al., Nat. Water 2 (2024) 674–683.
[26] T.H. Tsai, H.W. Chou, Y.F. Wu, Sep. Purif. Technol. 251 (2020) 117315.
[27] L. Liu, H. Lan, Y. Cui, et al., Sci. Adv. 10 (2024) eadn8696.
[28] P. Zhang, P. Li, Y. Ping, et al., Sci. Total Environ. 952 (2024) 175889.
[29] L. Zhou, J. Zhou, Y. Dong, et al., J. Hazard. Mater. 477 (2024) 135236.
[30] I. Elghamry, M. Gouda, Y.S.S. Al-Fayiz, Polymers 15 (2023) 1421.
[31] W.B. Elsharkawy, Fuller. Nanotub. Car. Nanostructures 32 (2024) 1005–1016.
[32] S.R. Al-Mhyawi, J. Mater. Res. Technol. 22 (2023) 3058–3074.
[33] K. Gupta, P. Joshi, R. Gusain, et al., Coord. Chem. Rev. 445 (2021) 214100.
[34] Y. Shi, S.T. Zhong, X. Wang, et al., Water Policy 24 (2022) 1590–1609.
[35] M. Vakili, Sep. Purif. Technol. 224 (2019) 373–387.
[36] D. Dou, J. Hazard Mater. 423 (2022) 127137.
[37] M.D. Silva, G. Cao, K.C. Tam, Environ. Sci.: Nano 12 (2025) 2154–2176.
[38] G. Lin, B. Zeng, J. Li, et al., Chem. Eng. J. 460 (2023) 141710.
[39] F.A. Alharthi, A.A. Abutaleb, M.M. Aljohani, et al., Comment. Inorg. Chem. 45 (2025) 245–282.
[40] F. Yuan, D.F. Yan, S.B. Song, et al., Chem. Eng. J. 506 (2025) 160063.
[41] L.L. Du, X. Li, X.F. Lu, et al., Sci. Total Environ. 939 (2024) 173478.
[42] S.W. Lv, J.M. Liu, Z.H. Wang, et al., J. Environ. Sci. 80 (2019) 169–185.
[43] A. Jamshaid, A. Hamid, N. Muhammad, et al., ChemBioEng Rev. 4 (2017) 240–256.
[44] R. Si, J. Pu, H. Luo, et al., Polymers 14 (2022) 5479.
[45] Y.Y. Jin, Y.N. Luan, Y.C. Ning, et al., Appl. Sci. 8 (2018) 1336.
[46] Y.F. Liu, C.W. Hu, G.P. Yang, Chin. Chem. Lett. 34 (2023) 108097.
[47] Y.F. Liu, Q.L. Hu, X.J. Chen, et al., Rare Metals 43 (2024) 1316–1322.
[48] C. Yang, J. Zhang, G. Yu, et al., Adv. Energy Mater. 15 (2025) 2403713.
[49] X.X. Li, D. Zhao, S.T. Zheng, Coord. Chem. Rev. 397 (2019) 220–240.
[50] T.T. Wang, Y.M. Ju, Y. Cheng, et al., Chin. Chem. Lett. 36 (2025) 109871.
[51] G.P. Yang, Y.F. Liu, K. Li, et al., Chin. Chem. Lett. 31 (2020) 3233–3236.
[52] Y. Liu, G. Zeng, Y. Cheng, et al., Chin. Chem. Lett. 35 (2024) 108480.
[53] R.Y. Zhou, Y. Liao, H.Z. Xu, et al., Chem. Eng. J. 512 (2025) 162335.
[54] Y. Jiang, C.J. Chen, K. Li, et al., Chem. Commun. 61 (2025) 4881–4896.
[55] H.N. Wang, X. Meng, Y.T. Cao, Small 21 (2025) 202408884.
[56] C.H. Zhang, J. Wang, J.Y. Zhan, et al., Chin. Chem. Lett. 36 (2025) 109719.
[57] M.L. Liu, X. Han, W.W. He, et al., Tungsten 6 (2024) 454–464.
[58] T. Bao, Y. Wu, C.C. Tang, et al., Adv. Mater. 37 (2025) 2500399.
[59] K. Yan, Z.H. Yu, Y.Y. Wang, et al., ChemSusChem 18 (2025) e202401456.
[60] Z.X. Sun, R. Wang, I.V. Kozhevnikov, Coord. Chem. Rev. 524 (2025) 216304.
[61] D. Pakulski, A. Gorczyński, D. Brykczyńska, et al., Angew. Chem. Int. Ed. 62 (2023) e202305239.
[62] R. Xue, Y.S. Liu, M.Y. Wang, et al., Mater. Horiz. 10 (2023) 4710.
[63] M. Lu, M. Zhang, J. Liu, et al., J. Am. Chem. Soc. 144 (2022) 1861–1871.
[64] G.P. Yang, J.W. Cao, Z.F. Lin, et al., Inorg. Chem. Front. 12 (2025) 1831–1838.
[65] M.A. Fashapoyeh, S. Shokrollahzadeh, A.M. Isloor, et al., Int. J. Biol. Macromol. 311 (2025) 143738.
[66] S. Wang, X.L. Geng, Z.Y. Zhao, et al., Water Res. 272 (2025) 122939.
[67] N. Aramesh, A. Reza Bagheri, Z. Zhang, et al., Coord. Chem. Rev. 507 (2024) 215767.
[68] X.L. Wang, L. Yang, Z. Zhang, et al., CrystEngComm 26 (2024) 1363–1370.
[69] H. Ullah, T.S. Alomar, S. Hussain, Microchem. J. 204 (2024) 110941.
[70] A. Troupis, A. Hiskia, H. Papaconstantinou, Environ. Sci. Technol. 36 (2002) 5355–5362.
[71] A. Ebrahimi, L. Krivosudsky, A. Cherevan, Coord. Chem. Rev. 508 (2024) 215764.
[72] J. Du, Y.Y. Ma, H.Q. Tan, Chinese J. Catal. 42 (2021) 920–937.
[73] H. Zhang, W.L. Zhao, H. Li, et al., Polyoxometalates 1 (2022) 9140011.
[74] A. Yoshida, Y. Nakagawa, K. Uehara, et al., Angew. Chem. Int. Ed. 48 (2009) 7055–7058.
[75] M. Barsukova-Stuckart, N.V. Izarova, R.A. Barrett, et al., Inorg. Chem. 51 (2012) 13214–13228.
[76] X.T. Xu, Y.F. Guo, B.L. Li, et al., Coord. Chem. Rev. 522 (2024) 216210.
[77] G.P. Yang, Y.F. Liu, Y.G. Wei, Coord. Chem. Rev. 521 (2024) 216172.
[78] H.X. Bi, M.S. Guo, J. Du, et al., Coord. Chem. Rev. 518 (2024) 216092.
[79] F.Q. Wang, Y. Zhang, W.W. Wang, Tungsten 7 (2025) 80–87.
[80] G.P. Yang, J.W. Cao, Y. Xiao, et al., Inorg. Chem. 64 (2025) 1041–1047.
[81] Y. Chu, X.H. Li, Z. Zhang, et al., Chin. Chem. Lett. 27 (2025) 111012.
[82] M. Xing, X.Y. Ji, S.X. Liu, Tungsten 6 (2024) 529–535.
[83] Y. Cheng, W.X. Shi, Z.M. Zhang, et al., Chin. Chem. Lett. 1 (2024) 110387.
[84] M.Y. Zhao, Q.Q. Liu, Y.Q. Feng, et al., Dalton Trans. 53 (2024) 18083–18088.
[85] H.T. Cui, T. Liu, M.L. Yang, et al., J. Mater. Chem. C 12 (2024) 11712–11722.
[86] H.Q. Liu, J.W. Cao, W. Tang, et al., Rare Metals 44 (2025) 3995–4002.
[87] X. Li, Hai, K. Guo, S.C. Chai, et al., Chin. Chem. Lett. 12 (2024) 110750.
[88] B. Hu1, Q.C. Du, Y. Yang, et al., Polyoxometalates 4 (2025) 9140079.
[89] C.H. Dong, X.N. Liu, Z. Li, et al., Adv. Funct. Mater. 35 (2025) 2418410.
[90] Y.J. Hao, T. Ji, J. Zhang, et al., Nano Res. 18 (2025) 94907192.
[91] Q. Zhu, Z.H. Li, T. Zheng, et al., Angew. Chem. Int. Ed. 64 (2024) e202413594.
[92] Z.Y. Gao, G.P. Yang, J. Dong, et al., J. Catal. 429 (2023) 115261.
[93] B.X. Zeng, G.P. Liu, M.J. Zhou, et al., Chem. Eng. J. 509 (2025) 161375.
[94] Z. Dong, S. Hu, Z. Li, et al., Small 19 (2023) 2300003.
[95] T. Chen, K. Yu, C. Dong, et al., Coord. Chem. Rev. 467 (2022) 214615.
[96] Y. Xie, Z.Y. Liu, Y.Y. Geng, et al., Chem. Soc. Rev. 52 (2023) 97–162.
[97] Y. Zhang, Y. Wang, Z. Dong, et al., Nat. Commun. 15 (2024) 9124.
[98] J. Li, Y. Zhao, B. Li, et al., Sci. China Chem. 68 (2025) 4348–4357.
[99] H. Liu, Q. Yang, N. Luan, et al., Nat. Sustain. 8 (2025) 553–561.
[100] Z.S. Chen, J.Y. Wang, M.J. Hao, et al., Nat. Commun. 14 (2023) 1106.
[101] L. Feng, Y. Yuan, B. Yan, et al., Nat. Commun. 13 (2022) 1389.
[102] Y. Yuan, D.D. Cao, F.C. Cui, et al., Nat. Water 3 (2025) 89–98.
[103] X. Liu, Y. Xie, M. Hao, et al., Nat. Commun. 15 (2024) 7736.
[104] C.M. Wen, Y.J. Yao, L.Y. Meng, et al., Ind. Eng. Chem. Res. 62 (2023) 18230–18250.
[105] J. Yu, H. Zhang, Q. Liu, et al., Chem. Eng. J. 471 (2023) 144705.
[106] H. Yang, M. Hao, Y. Xie, et al., Angew. Chem. Int. Ed. 62 (2023) e202303129.
[107] Y. Wu, Y.H. Xie, X.L. Liu, et al., Coord. Chem. Rev. 483 (2023) 215097.
[108] Q. Zhu, Z.H. Li, T. Zheng, et al., Angew. Chem. Int. Ed. 64 (2025) e202413594.
[109] B. Li, X.Z. Duan, Y.Z. Cui, et al., Angew. Chem. Int. Ed. 63 (2024) e202408096.
[110] M.Z. Chi, J.Y. Wei, Z.C. Zhao, et al., Angew. Chem. Int. Ed. 64 (2025) e202424499.
[111] Q. Zhao, Y. Zeng, Z. Jiang, et al., Angew. Chem. Int. Ed. 64 (2025) e202421132.
[112] Y.H. Hu, Y.Y. Wang, J.W. Zhao, et al., Coord. Chem. Rev. 506 (2024) 215724.
[113] Y. Liang, H.Y. Zhang, M.T. Huo, Adv. Mater. 37 (2025) 2415545.
[114] Q.X. Zhao, Y. Zeng, Z.Q. Jiang, et al., Angew. Chem. Int. Ed. 64 (2025) e202421132.
[115] S. Guo, C.W. Pan, M. Hou, et al., Angew. Chem. Int. Ed. 64 (2025) e202420398.
[116] P.H. Shi, X.M. Wang, H.L. Zhang, et al., ACS Appl. Mater. Interfaces 14 (2022) 54423–54430.
[117] Y.Y. Dong, Z.M. Dong, Z.B. Zhang, et al., ACS Appl. Mater. Interfaces 9 (2017) 22088–22092.
[118] X.W. Han, Y.Q. Wang, X.H. Cao, et al., Appl. Surf. Sci. 484 (2019) 1035–1040.
[119] D.Y. Du, J.S. Qin, S.L. Li, et al., Chem. Soc. Rev. 43 (2014) 4615–4632.
[120] X. Zhang, L.Y. Li, D.D. Shao, Sep. Purif. Technol. 302 (2022) 122154.
[121] H. Zhang, J.H. Xue, N. Hu, et al., Radioanal. Nucl. Chem. 308 (2016) 865–875.
[122] W. Yao, H.F. Xing, S. Ni, et al., J. Hazard. Mater. 480 (2024) 135985.
[123] Z.B. Zhang, Z.F. Li, Z.M. Dong, et al., Chin. Chem. Lett. 33 (2022) 3577–3580.
[124] Z.M. Dong, D.L. Zeng, Z.F. Li, et al., Chem. Sci. 15 (2024) 19126.
[125] R.X. Bi, X. Liu, Z.H. Peng, et al., Sep. Purif. Technol. 330 (2024) 125333.
[126] H.L. Zhang, W. Liu, A. Li, et al., Wang, Angew. Chem. Int. Ed. 58 (2019) 16110–16114.
[127] Y.L. Yang, K.K. Guo, X. Bai, et al., Inorg. Chem. Front. 12 (2025) 261–272.
[128] Y. Liu, D.H. Cui, T.T. Zhang, et al., Chem. Eng. J. 497 (2024) 154416.
[129] H.L. Guo, E. Hu, Y.H. Wang, et al., Nat. Commun. 16 (2025) 2012.
[130] H.L. Zhang, A. Li, K. Li, et al., Nature 616 (2023) 482–487.
[131] S.J. Xie, Green Chem. Lett. Rev. 17 (2024) 2357213.
[132] H. Xiang, S. Yao, A. Zhang, et al., J. Water Process Eng. 69 (2025) 106762.
[133] X.R. Tian, X. Xin, Y.Z. Gao, et al., Acta Cryst. C74 (2018) 1310–1324.
[134] Q. Cen, W. Xiao, Y.Q. Liu, et al., Chem. Res. Chin. Univ. 36 (2020) 1128–1135.
[135] J.Q. Niu, W.T. An, X.J. Zhang, et al., Chem. Eng. J. 418 (2021) 129408.
[136] X. Xin, N. Hu, Y.Y. Ma, et al., Dalton Trans. 49 (2020) 4570–4577.
[137] Y.L. Wang, Y.Y. Ma, Q. Zhao, et al., Sens. Actuators B: Chem. 305 (2020) 127469.
[138] X.Y. Ma, H.X. Bi, X.J. Zhang, et al., Polyoxometalates 4 (2025) 9140090.
[139] X.T. Wang, W.J. Mao, D.S. Wang, et al., Talanta 257 (2023) 124270.
[140] Q.Q. Liu, X.L. Wang, H.Y. Lin, et al., Dalton Trans. 50 (2021) 9450–9456.
[141] D.L. Tang, Z. Xiong, P. Lu, et al., Chem. Eng. Sci. 262 (2022) 118003.
[142] F. Zou, R.H. Yu, R.G. Li, et al., ChemPhysChem 14 (2013) 2825–2832.
[143] H.X. Wang, Z.L. Liu, B. Zhao, et al., Microchem. J. 195 (2023) 109505.
[144] K.M. Pan, H. Ming, Y. Liu, et al., New J. Chem. 36 (2012) 113–118.
[145] Q. Jiang, K. Zhu, Nat. Rev. Mater. 9 (2024) 399–419.
[146] Q.X. Zhuang, Z.Y. Xu, H.Y. Li, et al., Sci. Adv. 11 (2025) eado7318.
[147] B.Y. Hu, J. Zhang, Y.L. Yang, et al., Chin. Chem. Lett. 35 (2024) 108933.
[148] Y.Y. Dong, J. Zhang, Y.L. Yang, et al., Nano Energy 97 (2022) 107184.
[149] Y.Y. Dong, J. Zhang, W. Wang, et al., Small 19 (2023) 2301824.
[150] H. Fakhri, A.R. Mahjoub, H. Aghayan, J. Radioanal. Nucl. Chem. 321 (2019) 449–461.
[151] Y.X. Liu, P.X. Wu, J.Y. Dai, et al., Nat. Commun. 15 (2024) 8896.
[152] H. Ullah, T.S. Alomar, M. Tariq, et al., J. Environ. Chem. Eng. 12 (2024) 114257.
[153] H. Ullah, T.S. Alomar, S. Hussain, et al., Microchem. J. 204 (2024) 110941.
[154] S. Herrmann, L.D. Matteis, J.M.D.L. Fuente, et al., Angew. Chem. Int. Ed. 56 (2017) 1667–1670.
[155] H. Zhang, M. Li, Z.L. Liu, et al., J. Mol. Struct. 1267 (2022) 133604.
[156] M. Kahloul, S. Mahfoudhi, I. Ounifi, et al., Water Sci. Technol. 86 (2022) 1510–1526.
[157] C.A. Nagasaka, N. Ogiwara, S. Kobayashi, et al., Small 20 (2024) 2307004.
[158] N. Tamai, N. Ogiwara, E. Hayashi, et al., Chem. Sci. 14 (2023) 5453–5459.
[159] S. Seino, R. Kawahara, Y. Ogasawara, et al., Angew. Chem. 128 (2016) 4055–4059.
[160] K. Li, T. Liu, J. Ying, et al., Dyes Pigm. 222 (2024) 111898.
[161] D. Zhou, Z. Li, Y. Chen, et al., Angew. Chem. Int. Ed. 64 (2025) e202502751.
[162] Z.H. Huo, B. Akhsassi, J.M. Yu, et al., Inorg. Chem. 64 (2025) 3371–3383.